The "Dashpot" Mechanism of Stretch-dependent Gating in MscS

Bradley Akitake, Andriy Anishkin, and Sergei Sukharev

Department of Biology, University of Maryland, College Park, MD 20742

ABSTRACT The crystal structure of the small conductance mechanosensitive channel (MscS) has been an invaluable tool in the search for the gating mechanism, however many functional aspects of the channel remain unsettled. Here we characterized the gating of MscS in *Escherichia coli* spheroplasts in a triple mutant (*mscL*$^-$, *mscS*$^-$, *mscK*$^-$) background. We used a pressure clamp apparatus along with software developed in-lab to generate dose–response curves directly from two-channel recordings of current and pressure. In contrast to previous publications, we found that MscS exhibits essentially voltage-independent activation by tension, but at the same time strong voltage-dependent inactivation under depolarizing conditions. The MscS activation curves obtained under saturating ramps of pressure, at different voltages, gave estimates for the energy, area, and gating charge for the closed-to-open transition as 24 kT, 18 nm^2, and +0.8, respectively. The character of activation and inactivation was similar in both K^+ and Na^+ buffers. Perhaps the most salient and intriguing property of MscS gating was a strong dependence on the rate of pressure application. Patches subjected to various pressure ramps from 2.7 to 240 mmHg/s revealed a midpoint of activation almost independent of rate. However, the resultant channel activity was dramatically lower when pressure was applied slowly, especially at depolarizing pipette voltages. It appears that MscS prefers to respond in full to abrupt stimuli but manages to ignore those applied slowly, as if the gate were connected to the tension-transmitting element via a velocity-sensitive "dashpot." With slower ramps, channels inactivate during the passage through a narrow region of pressures below the activation midpoint. This property of "dumping" a slowly applied force may be important in environmental situations where rehydration of cells occurs gradually and release of osmolytes is not desirable. MscS often enters the inactivated state through subconducting states favored by depolarizing voltage. The inactivation rate increases exponentially with depolarization. Based on these results we propose a kinetic scheme and gating mechanism to account for the observed phenomenology in the framework of available structural information.

KEY WORDS: mechanosensitive channel • voltage • tension • inactivation • osmoregulation

INTRODUCTION

MscS is a major component of the turgor regulation system in bacteria that also includes the large channel MscL (Blount and Moe, 1999; Levina et al., 1999). These two osmotic "valves" activate at different tension thresholds, providing a graded permeability response to osmotic down-shifts of varied magnitude. Efflux of osmolytes through these channels reduces the osmotic pressure and effectively protects the bacterial cells against lysis. Each of these molecules, MscS and MscL, forms a gigantic pore in the membrane gated directly by tension in the surrounding lipid bilayer. Despite having no sequence homology or structural similarity, a unique functional convergence and even partial redundancy (Levina et al., 1999) makes these two channels especially interesting for basic studies of mechanotransduction. MscS and MscL represent advanced systems that may reveal how common biophysical principles of gating are implemented with dissimilar structural designs. In contrast to MscL, which is a strictly prokaryotic molecule, MscS homologues are more abundant, having also been found in eukaryotes, increasing the value of MscS as a model (Pivetti et al., 2003).

Martinac and coworkers (Martinac et al., 1987), who were the first to apply patch-clamp techniques to giant *Escherichia coli* spheroplasts, reported a pressure-gated bacterial channel of 1 nS conductance. MscS, a mechanosensitive channel with 1-nS conductance was identified later as a product of the orphan *yggB* gene, sharing similarity with the NH_2-terminal half of the potassium efflux protein MscK (formerly KefA) (Levina et al., 1999). MscK was also shown to be a mechanosensitive channel with conducting characteristics similar to that of MscS (Levina et al., 1999). However, while MscS exhibited time-dependent inactivation (Koprowski and Kubalski, 1998; Levina et al., 1999), MscK was characterized by more sustained activities under constant stimulation. MscK gating was also found to be critically dependent on the presence of potassium ions in the external medium (Li et al., 2002).

Crystallographic work by the Rees group recently produced the crystal structure of *E. coli* MscS (Bass et al., 2002), revealing a homo-heptameric complex with three transmembrane helices per subunit and a large cytoplasmic COOH-terminal domain. Two transmembrane helices M1 and M2 were bundled together, resembling

Correspondence to Sergei Sukharev: sukharev@umd.edu

J. Gen. Physiol. © The Rockefeller University Press • 0022-1295/2005/02/143/12 $8.00
Volume 125 February 2005 143–154
http://www.jgp.org/cgi/doi/10.1085/jgp.200409198

the "paddle" of the KvAP voltage sensor (Jiang et al., 2003). Due to the presence of several arginines, these helices were proposed to serve a similar function as the MscS voltage sensor. The third transmembrane helix (M3) lined a relatively wide but very hydrophobic pore, deemed to represent the open conformation (Bass et al., 2002). Our computational studies suggested that the MscS pore constriction is dehydrated and likely nonconductive (Anishkin and Sukharev, 2004), thus raising the question of what functional state the crystal structure actually represents. Independent computational studies also confirmed the dehydrated and low-conducting nature of the MscS pore (Sotomayor and Schulten, 2004). Biochemical cross-linking experiments suggested that the native closed conformation of the channel is more compact as compared with the crystal conformation in both the transmembrane and cytoplasmic domains (Miller et al., 2003).

The available molecular information on MscS facilitates tremendously many aspects of functional studies. While cloning and tagging of MscS permitted purification and functional reconstitution of the protein in liposomes (Okada et al., 2002; Sukharev, 2002), generation of the MJF465 triple mutant (*mscL*$^-$, *mscS*$^-$, *mscK*$^-$) *E. coli* strain prepared a "clean" genetic background on which the channel could be studied it its native setting (Levina et al., 1999). The first brief report of MscS behavior at different voltages measured in a clean system (Vasquez and Perozo, 2004) gave a different picture of gating compared with the previous phenomenology (Martinac et al., 1987; Koprowski and Kubalski, 1998) collected on mixed channel populations.

The present work characterizes the behavior of MscS in the MJF465 triple mutant *E. coli* strain (Levina et al., 1999). Data collection was aided by a high-speed pressure clamp apparatus to deliver reproducible ramps of pressure to patches. Software developed in-lab allowed us to generate dose–response curves directly from the resulting two-channel recordings of current and pressure. The results indicate that MscS activation is essentially voltage independent, however the net channel activity is strongly influenced by the process of reversible inactivation. MscS inactivation was found to be both tension and voltage dependent. The interplay of these two processes, activation and inactivation, makes MscS most responsive to abruptly applied mechanical stimuli. We propose a kinetic scheme and gating mechanism in an attempt to reconcile the observed phenomenology with the crystal structure.

MATERIALS AND METHODS

Strains

Analysis of MscS was performed in giant *Escherichia coli* spheroplasts as described by Martinac et al., 1987. The PB111 construct containing the *mscS* gene under the control of an inducible P_{lacUV5} promoter was provided by P. Blount (University of Texas, Dallas, TX). The expressed channel protein has a COOH-terminal 6His tag, which was shown previously to have little effect on the character of gating in the absence of His-binding divalent ions (Koprowski and Kubalski, 2003). For electrophysiological analysis, the construct was electroporated into the MJF465 (*mscL*$^-$, *mscS*$^-$, *mscK*$^-$) triple knock-out strain, a gift from I.R. Booth (University of Aberdeen, Aberdeen, UK). All analyses were repeated in at least two independent spheroplast preparations.

Electrophysiology

Patch-clamp recordings of MscS were taken in an excised patch, voltage clamp, configuration on an Axon 200B amplifier attached to an Axon DigiData 1320A A/D converter (Axon Instruments). Electrodes were borosilicate capillaries pulled to a bubble number of 4.5 (resistance 2.8 ± 0.2 MΩ, in a buffer of 39 mS/cm conductivity) on a micropipette puller (Sutter Instruments Company). Recording was performed in symmetrical potassium (200 mM KCl, 90 mM $MgCl_2$, 10 mM $CaCl_2$, 5 mM HEPES titrated to pH 7.4 with KOH) or sodium (replaces above KCl with 200 mM NaCl) buffers in the pipette. The bath solution differed only in the addition of 300 mM sucrose. Pressure ramps were applied using an HSPC-1 high-speed pressure clamp apparatus (Besch et al., 2002) controlled via analogue output from the DigiData1320A. ALA Scientific Instruments' P-V Pump unit was used as the pressure and vacuum source. Vacuum and pressure were calibrated at both the pumps and the headstage using a PM015D pressure monitor (World Precision Instruments). Pressure traces were then recorded directly from the HSPC-1 head stage. Output commands to the HSPC-1 were controlled by Axon pClamp8 software in episodic stimulation mode (Axon Instruments).

Data Collection and Treatment

Axon pClamp 8 software was used to record the integral current through patches with a bandwidth of 1–5 kHz, digitizing at 1,000–2,5000 samples/s depending on the duration of the recording. Two-channel (current and pressure vs. time) electrophysiological recordings were converted into Axon Text Format and subsequently analyzed using HISTAN, software custom-written in Matlab. A dose–response curve (P_o/P_c vs. pressure) calculation was implemented using the following protocol. The whole pressure range was divided into bins of 1 mm Hg width and all-point current histograms were created for each pressure value. Following baseline correction, an average integral current value I(p) was calculated for every pressure bin. An opening probability for the MscS population was estimated by $P_o(p) = I(p)/I_{max}$, where I_{max} represents the maximal integral current observed in the recording. Under typical conditions (applied pipette voltage range of −30 to 80 mV), where the relative occupancy of subconducting states was very low, this approach gave an adequate estimation of the open probability of MscS. However, out of this range, subconducting states are dominant and this approach provides only an approximation of P_o since it relies on an assumption that the contribution of the substates to integral current, relative to the fully open state, does not change significantly with tension. Proper treatment of MscS traces recorded at high positive and negative voltages will be a focus in future research.

Pressure to Tension Conversion

The midpoint pressure ($p_{1/2}^{20}$) at which half of the MscS population was activated under +20 mV during the fastest (1 s) pressure ramp was used as a tension calibration point. $p_{1/2}^{20}$ was calculated

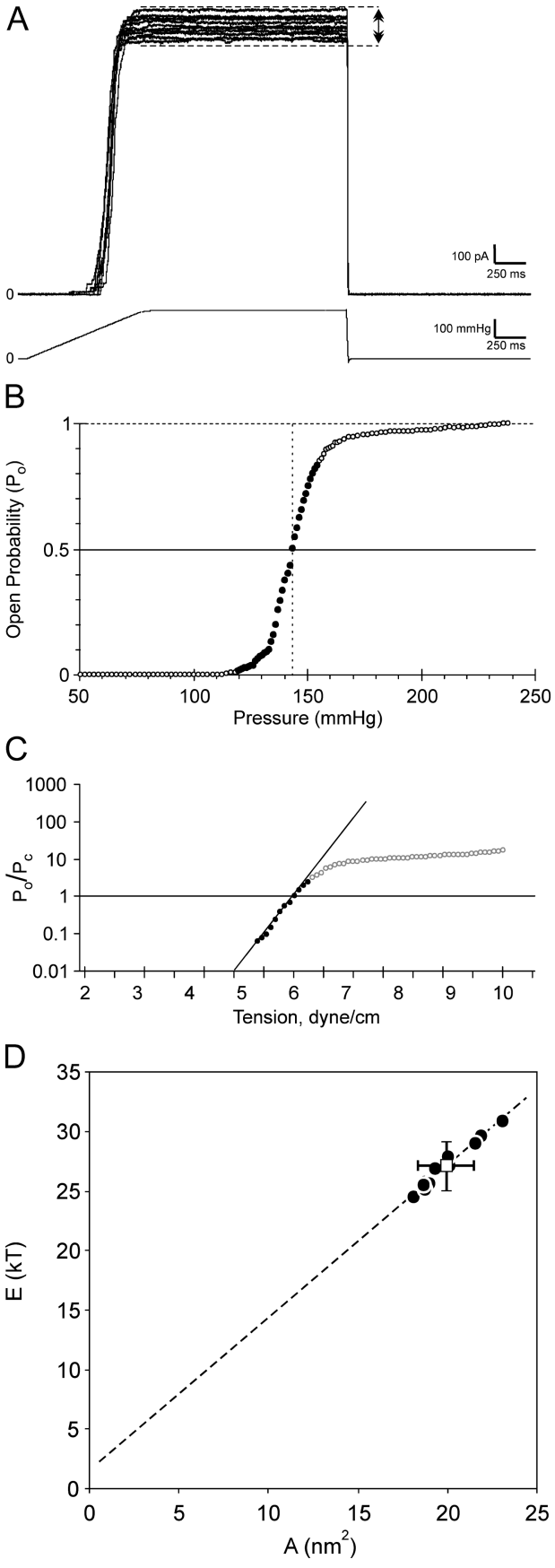

for each patch individually as an average of all traces recorded under a single applied voltage (usually 3–10 recordings). This average pressure corresponds to 5.5 dyne/cm, earlier shown to be the tension midpoint for MscS activation in spheroplasts (Cui and Adler, 1996) and liposomes (Sukharev, 2002). $p_{1/2}^{20}$ was then used in tension calculations for the remaining traces, recorded from the same patch, under different applied voltage. Pressures were converted to tensions using the law of Laplace for spherical surfaces: $\gamma = (p / p_{1/2}^{20}) \times 5.5$ dyne/cm. This conversion implies that in the range of pressure needed to activate MscS patch, geometry does not substantially change. Based on video observations of liposome patches (Sukharev et al., 1999), the membrane was found to be essentially flat at a zero pressure, becoming hemispherical under a pressure gradient. The curvature of liposome patches saturated with increasing pressures and remained stable in a range of tensions from 4–5 dyne/cm. These findings are likely true for spheroplast patches as well.

Fitting Procedures

Dose–response curves for MscS were fitted with a two-state Boltzmann-type model where

$$P_o/P_c = \exp[-(\Delta E - \gamma \Delta A)/kT]. \quad (1)$$

P_o and P_c are the probabilities for the open and closed states, ΔE is the difference in energy between the states in an unstressed membrane, ΔA is the in-plane protein area change during the gating transition, γ is the membrane tension, and kT has the conventional meaning (Sachs, 1992; Sukharev et al., 1999). Fitting was performed in Microsoft Excel 2000 using a linear least squares method in semilogarithmic coordinates ($\log(P_o/P_c)$ vs. tension). Only the first linear part of activation curve was fitted (see RESULTS), representing activation of the main population of MscS channels.

To characterize the time course of the MscS inactivation at constant pressure, the falling phase of the integral current was fitted with a single standard exponent of the first order ($I(t) = Ae^{-t/\tau} + C$, where I is an integral current, t time, A amplitude, C additive constant, and τ time constant). Fitting was performed in Axon Clampfit 9 using a Levenberg-Marquardt search method and sum of squared errors minimization criterion.

RESULTS

Activation Curves of MscS Measured with Reproducible Pressure Ramps

Membrane patches, excised from giant *E. coli* spheroplast expressing wild-type MscS, were exposed to 1-s linear ramps of pressure ending with a constant 2-s

FIGURE 1. Responses of MscS populations to a 1-s linear pressure ramp followed by a 2-s plateau. (A) Superimposed raw traces obtained in the same patch at +20-mV pipette voltage. Arrows represent variability in maximal current. (B) One trace from the dataset in A converted into a dose–response curve by plotting $P_o = I/I_{max}$ vs. pressure. (C) The P_o/P_c–tension dependence plotted in a semilogarithmic scale. The pressure scale was converted to tensions by equating the tension at the pressure midpoint (mean $p_{1/2}$ for all traces in A) to 5.5 dyne/cm and the linear part of the dependence was fitted with Eq. 1 (see MATERIALS AND METHODS). (D) Correlated distribution of ΔE vs. ΔA parameters extracted from the traces obtained in the same patch (A).

plateau of saturating pressure. Fig. 1 A shows seven superimposed traces from one representative patch, recorded under a +20 mV pipette voltage. When the saturating pressure was reached, the current through the open channel population achieved some maximal level. As shown below, various factors such as the rate of pressure application, or preactivation of the population with nonsaturating pressure steps, altered that final level. However, even when the stimulation conditions were kept constant, there was still some variability in maximal current under repeated activation (Fig. 1 A). This base variability, with large channel populations (20 or more channels per patch), was consistently ~10% (Fig. 1 A, arrows), when provided with a 3-min "rest" period at 0 mV between pressure applications. Reducing the time between pressure ramps significantly decreased the final current, indicating that prior treatment changes the availability of channels by driving a part of the population to an inactive state. The population also showed decreased maximal current if the patch was kept under depolarizing (pipette negative) potentials during the "rest" period. A 3-min interval between stimuli under low positive or zero applied voltage generally allowed the population to fully recover. Despite this variability of maximal current, the pressure midpoint (pressure of half maximal activation of MscS, $p_{1/2}$) of MscS channels activated by sequential pressure ramps was more consistent, varying within 1.6% of the mean. Among five representative patches studied with standard borosilicate pipettes (see MATERIALS AND METHODS), the average $p_{1/2}$ was 188 ± 31 mm Hg, which can be accounted for by differences in pipette size and patch geometry.

Using HISTAN software, dose–response curves of open probability (P_o) versus pressure were generated using a two-dimensional histogram approach (Chiang et al., 2004) directly from two-channel recordings of current and pressure (Fig. 1 B). The maximal current (I_{max}) during each pressure application was taken to represent the highest open probability ($P_o = 1$) and all other current points were normalized to it, producing $P_o = I/I_{max}$. Maximal current was estimated to be the highest level achieved in each separate pressure application. Assuming a tension midpoint ($\gamma_{1/2}$) for MscS of 5.5 dyne/cm (Sukharev, 2002) at +20 mV, pressure dependencies were converted to $P_o/P_c(\gamma)$ and fit with a two-state Boltzmann equation to extract apparent (ΔE) and area (ΔA) for the opening transition (Fig. 1 C). Analysis of many patches indicated nonuniformity in the MscS population, with a "main" population whose P_o/P_c ratio depended strongly on tension and a second, much smaller, "late" population that activated with a lower slope on pressure. Part of this late population had a delayed behavior, activating after the ramp reached its plateau. The contribution of the late population ranged from 0 to 5% of the total integral current, therefore only the linear portion of the activation curve was fitted and used for determination of the overall gating parameters (Fig. 1 C).

Values of ΔE and ΔA for the MscS gating transition, extracted from sequential ramps applied to the patch shown in Fig. 1 A, averaged 27 ± 2 kT and 20 ± 1.6 nm^2 respectively ($n = 11$). The combined values from five different patches taken from independent spheroplast preparations produced ΔE = 24 ± 4 kT and ΔA = 18 ± 3 nm^2 ($n = 27$). A plot of ΔE versus ΔA from the same patch (Fig. 1 D) illustrated strong correlation in the variation of these parameters. A previous study of population responses in MscL (Chiang et al., 2004) showed that slightly nonhomogeneous populations of channels display strong linear correlations of ΔE and ΔA. This appeared to be the case for MscS, where variation of the slope of the dose–response curves was substantially larger than variation in the midpoint position. Note that at the tension midpoint ($\gamma_{1/2}$), $P_o = P_c$, and therefore from Eq. 1 $\gamma_{1/2} = \Delta E/\Delta A$. Linearly correlated pairs of ΔE and ΔA arise from dose–response curves that intersect at the same $\gamma_{1/2}$ but have variation in their slopes. Statistical simulations of nonhomogeneous channel populations illustrated that the slope of the dose–response curves should be lower than that of an ideally homogeneous population. Furthermore, this slope reduction increases with the scatter of intrinsic parameters (ΔE and ΔA) characterizing each individual channel. If the source of nonhomogeneity is a deviation of the intrinsic parameters, then the values extracted directly from the activation curves represent lower bound estimates for ΔE and ΔA. If however the deviations of the dose–response curves are more related to the stochastic nature of crossing the transition barrier (which can produce variations in P_o under nonequilibrium pressure ramps) during the gating transition then these average values of ΔE and ΔA may closer reflect the true intrinsic parameters for MscS. Further analysis is required to fully explain the dose–response curve variability in the MscS channel population.

Voltage Dependence of MscS Activation

The same patch clamp experiments, with linear ramps of saturating pressure, were repeated at different voltages from −100 mV to +100 mV. The midpoint for MscS activation remained essentially constant at both high positive and moderate negative voltages as shown by the raw traces in Fig. 2 A. A similar character of currents was observed in both symmetrical KCl and NaCl-based buffers. In several independent experiments, the maximal conductance for each individual trace was normalized to that observed at +20 mV and plotted as a function of voltage (Fig. 2 B). The maximal conduc-

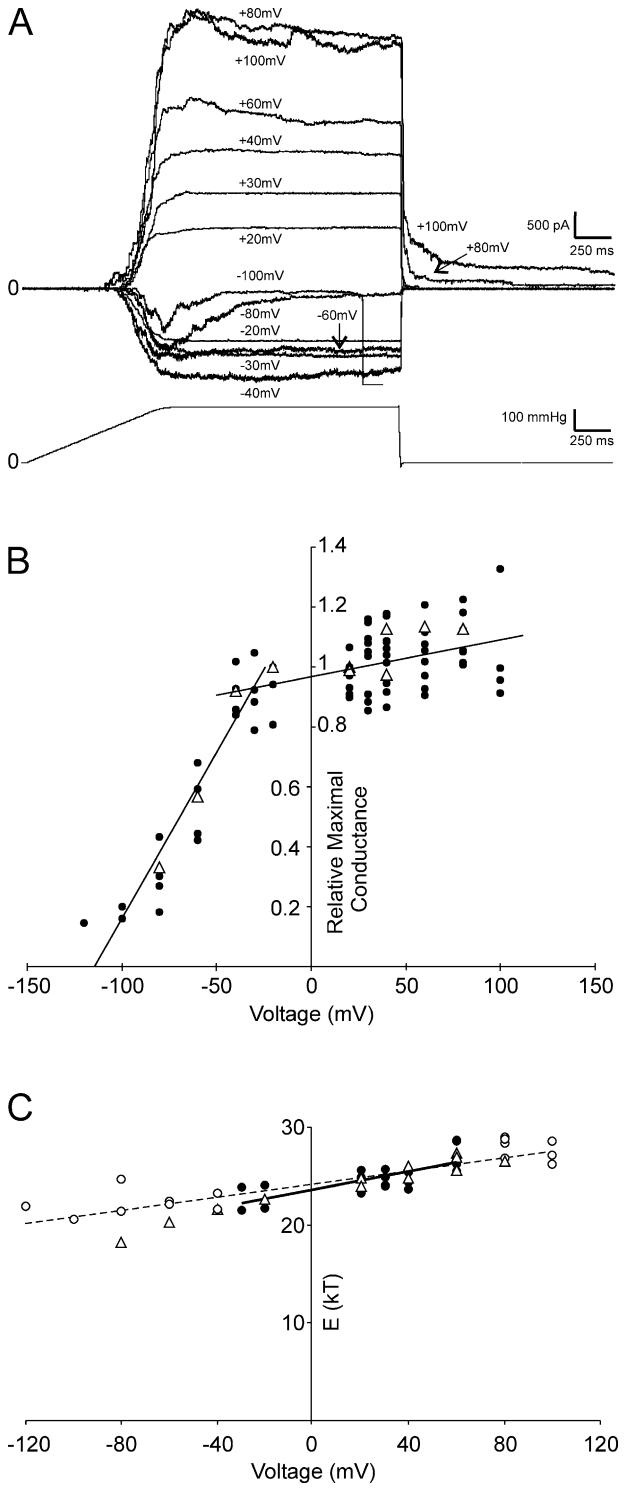

FIGURE 2. Responses of MscS populations to linear pressure ramps at different voltages. (A) Raw traces recorded at pipette voltages ranging from −100 to +100 mV (patch ruptures near the end of the −100-mV trace). Maximal conductance for the MscS population increases linearly with voltage in the range of moderate voltages (−30 to +40 mV). At high positive pipette voltages (>+60 mV), MscS behavior becomes more irregular and a population of channels remains open even after pressure has been released, increasing in number with higher voltages (right side, +80 and +100 mV). At very negative pipette voltages (<−40 mV), there is clear break in the modality of the traces as inactivation becomes prominent. (B) Maximum relative conductance as a function of voltage for four different patches. The data presented for KCl (closed circles) and NaCl (open triangles) recording buffers. (C) The energy of the closed-to-open transition (ΔE, fitted with the fixed $\Delta A = 17\ nm^2$) as a function of voltage, for three independent patches in KCl (circles) and NaCl (triangles).

tance at high positive pipette voltages (+60, +80, and +100 mV) increases shallowly. At negative pipette voltages, beyond −40 mV, a steep decrease of the integral patch conductance was obvious (Fig. 2 B). Traces were treated as described in the previous section (Fig. 1, B and C) and the effective parameters ΔE and ΔA were obtained for each voltage. The plot of ΔE versus voltage showed MscS activation to be only weakly dependent on applied electric field (Fig. 2 C). From the slope of the fit, gating charge (q) was determined to be +0.8 per MscS heptamer or about +0.1 per subunit. This small value for q indicates that the charges within the electric field, most of which lie on the lipid facing helices, do not displace significantly in the direction of electric field during MscS activation. Given that a net charge of +3.0 resides on each TM1–TM2 pair, the transmembrane movement of these helices would be no more than 0.7 Å.

In an attempt to explain the dramatically decreased integral conductance at negative pipette voltages, MscS activities were recorded from patches expressing a smaller number of channels. An analysis of the most frequently observed MscS single channel amplitudes versus voltage is shown in Fig. 3 A. The continuous line represents the fit of maximal current amplitudes, reflecting the conducting properties of the fully open state of MscS. The plot also reveals a pair of bifurcations (Fig. 3 A, dashed lines) taking place at +60 and −40 mV, signifying an increased presence of subconducting levels. Between these voltages, the contribution of substates was very small (∼3% of the open time, leading to 0.5% decrease in the integral current) and essentially tension independent. At higher voltages, both positive and negative, channels exhibited a preference for the lower conducting states. Fig. 3 B shows a typical trace obtained at a constant moderate pressure with four to five channels open. Reversal of the pipette voltage from +40 to −40 mV switched the character of gating. Channels that were fully open at +40 mV showed flickering in and out of substates at −40 mV. The substates display noticeably faster kinetics than the main closed to open transition. All of the MscS channels had inactivated by the end of the shown episode. The same experiment at +60 mV revealed that fully open channels at positive voltages immediately entered stable substates when voltage was reversed to −60 mV and also quickly inactivated (Fig. 3

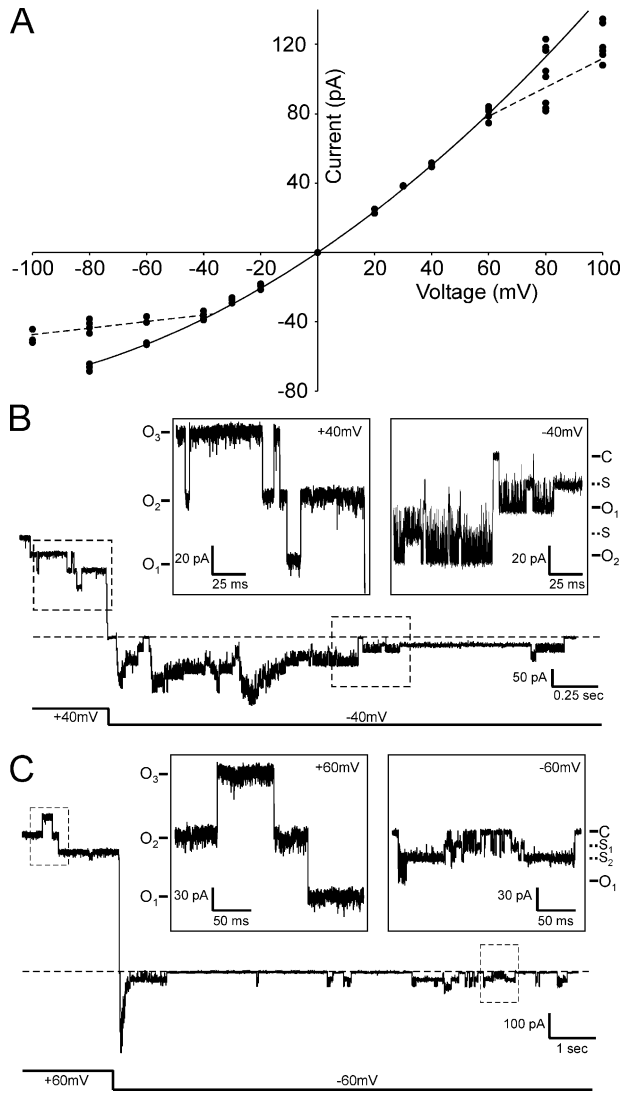

FIGURE 3. Single-channel conductance of MscS as a function of voltage and the occupancy of substates. (A) Frequently observed single-channel conductances plotted as a function of pipette voltage. The solid line is the fit of maximal values representing the fully open state of MscS. The "break" of the curve at −40 and +60 mV mark the points where substates become prominent. (B and C) Traces illustrating the changes in MscS gating upon switching pipette voltage from +40 to −40 mV (B) and from +60 to −60 mV (C). The magnified episodes illustrate full transitions at positive pipette voltages and switching to subconducting states and inactivation at negative.

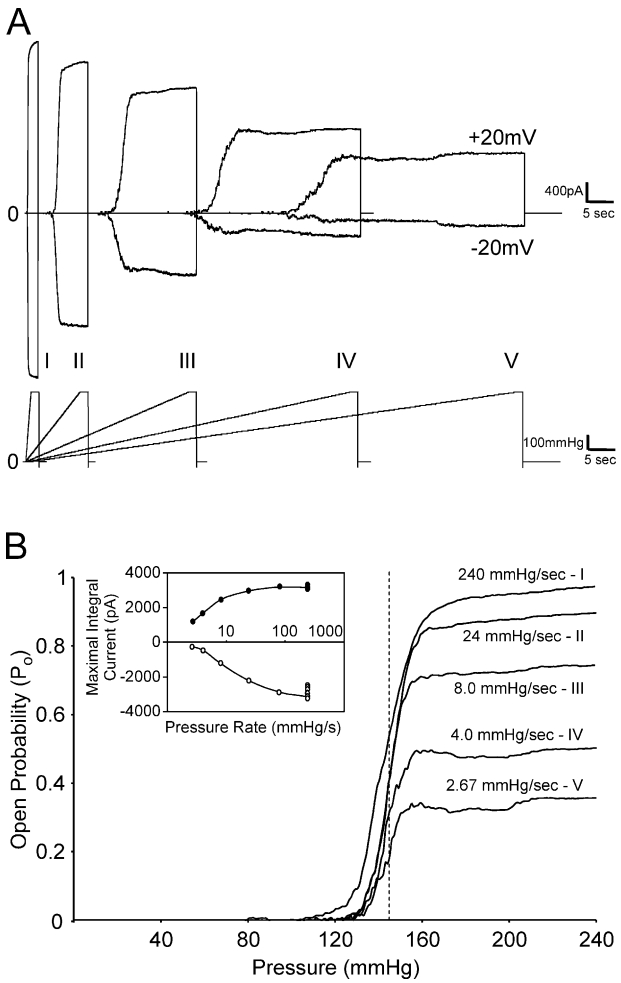

FIGURE 4. MscS responses to ramps applied at different rate. (A) Raw current traces (top) recorded at pipette voltages of +20 and −20 mV under pressure ramps varying from 2.7 to 240 mm Hg/s (bottom). (B) Activation curves for different ramps ($P_o = I/I_{max}$, where I_{max} is scored at fastest ramp) presented in one scale as a function of pressure. Inset, maximum current as a function of rate at positive and negative voltages.

C). Substates coincident with inactivation suggest that at negative voltages, inactivation proceeds through these lower conducting substates. The increased occupancy of substates and inactivation seen in the single-channel traces explains the decline of the integral current observed in multichannel patches at high negative voltages (Fig. 2 B). The small positive slope of the maximal integral conductance observed at positive pipette voltages likely reflects the slightly rectifying nature of the fully open state.

Availability of MscS Depends on the Rate of Pressure Application and the Amplitude of Prepulse Pressure

To investigate the dynamics of MscS responses to stimuli applied with different rates, patches were subjected to various ramps of pressure ranging from 2.7 to 240 mm Hg/s. Raw traces of current aligned with the pressure ramps in Fig. 4 A show that the resultant channel activity at the end of the ramp was dramatically lower when pressure was applied slowly, especially at negative pipette voltages. Conversion of traces into $P_o(p)$ dependencies (Fig. 4 B) revealed $p_{1/2}$ of MscS activation to be almost independent of rate. Similarly, a plot of the intrinsic gating parameters ΔE and ΔA revealed no dependence on the rate of pressure application (unpublished data). An analysis of P_o, normalized to the fastest ramp, showed a monotonic dependence on the rate of pressure applica-

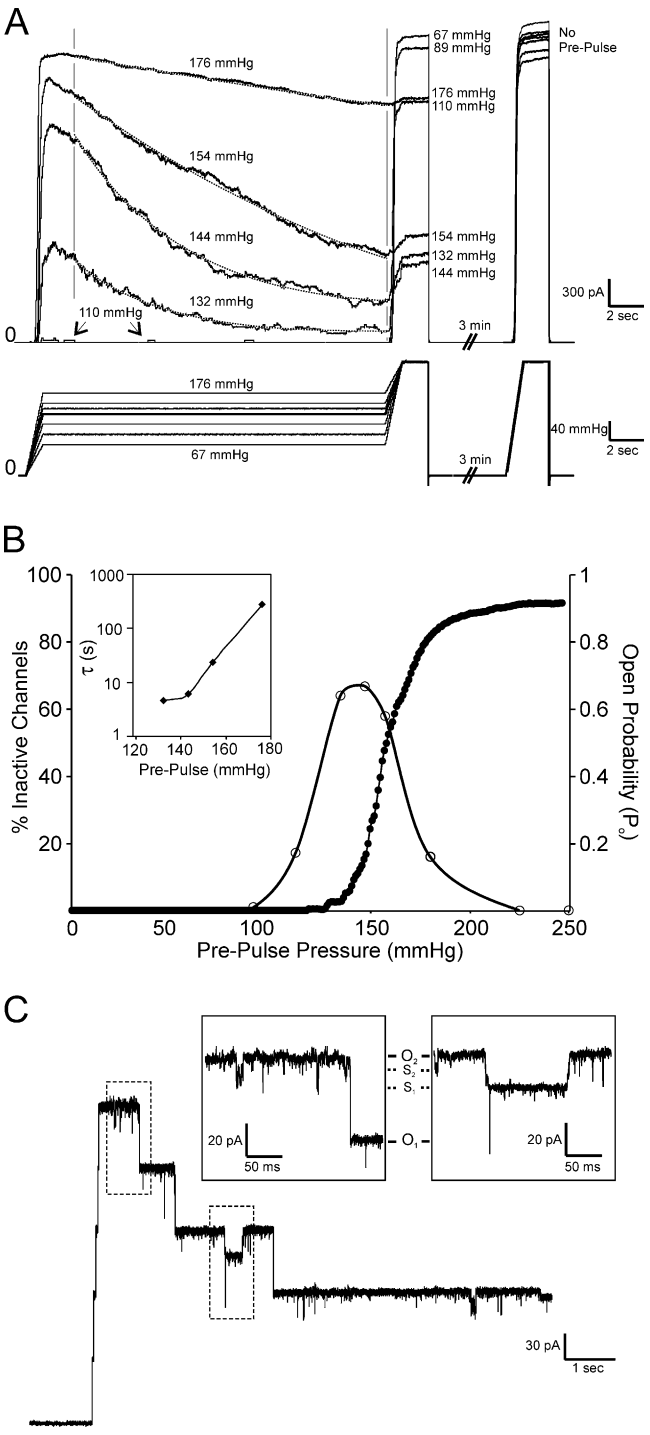

FIGURE 5. Dynamics of MscS response at intermediate pressures. (A) Raw traces obtained with 20-s pressure prepulses of different amplitude followed by shorter (2 s) test pulses of saturating pressure. The current kinetics during the prepulse reflects the rate of channel inactivation, whereas the response to the test pulse checks for the MscS availability after the prepulse. The process of inactivation was fitted by single exponents shown by dotted lines. (B) The fraction of MscS inactivated during the prepulse as a function of pressure (open circles); the activation ($P_o(p)$) curve is presented to show the position of the pressure midpoint for the same patch. Inset, the characteristic time of inactivation as a function of pressure. (C) A trace obtained at a pressure near the midpoint from a patch having only five channels. The magnified episodes show the presence of substates at low positive pipette voltages.

tion, with a lower maximal current for a slower ramp (Fig. 4 B, inset). At the slowest ramp speeds, noticeable oscillations appeared in the activation curves, suggesting that two competing processes, activation and inactivation, were superimposed. The net result is a reduction in the observed maximal conductance.

To obtain further insight as to why MscS responds in full to abrupt stimuli but tends to "dump" those applied more slowly, a two-step protocol was adopted. Patches were first exposed to a 20-s prepulse of intermediate pressure (nonsaturating) and then immediately to a short saturating pulse to sample channel availability (Fig. 5 A). The range of prepulse amplitudes was centered on the activation pressure midpoint ($p_{1/2}$). The results showed that the majority of channels enter the inactive state at "prepulse" pressures below $p_{1/2}$ (Fig. 5 B). In addition, raising the prepulse pressure significantly decreased the rate of channel inactivation (τ) derived from an exponential fit of the inactivation component (Fig. 5 B, inset). Saturating pressures or those substantially above $p_{1/2}$ tended to prevent channel inactivation, suggesting that the fully open conformation of MscS is stabilized by high membrane tensions. The decrease of inactivation rate signifies an increase of the energy difference between the open state and transition state separating the open from inactivated state. Assuming that the activation midpoint (Fig. 5 B) is 5.5 dyne/cm, the estimated area change suggests that the footprint of the channel complex decreases by 10.6 nm^2 as it approaches the transition barrier from the open state.

Single-channel inactivation events were resolved in smaller channel populations by preparing spheroplasts with no IPTG induction. Promoter "leakage" alone results in four to six MscS channels being observed in each patch. Higher resolution (10 kHz) recordings of inactivation at intermediate prepulse pressures in these patches showed that MscS visits substates even at positive pipette voltages (Fig. 5 C). However, a comparison reveals that the total occupancy of substates at positive voltages is substantially lower than its counterpart at negative voltages. At low voltages (both positive and negative), inactivation events appeared as straight transitions from the fully conductive to a nonconductive state without visible intermediates. The resolution of these recordings may still be insufficient to reject the possibility of short-lived intermediate states during low-voltage inactivation.

Inactivation is Favored by Depolarization

Experiments similar to those above, with a prepulse pressure slightly higher than $p_{1/2}$, were conducted at dif-

ferent pipette voltages. A comparison of these traces showed a clear increase in the rate of inactivation at negative potentials (Fig. 6 A). As previously described, the inactivation phase of each trace was fitted with an exponent, and characteristic times were determined. A plot of τ versus voltage (Fig. 6 B) exhibited a shallow increase between -40 and $+60$ mV, indicating that moderate positive pipette voltages oppose inactivation. A steep decrease of τ below -40 mV revealed the onset of strong MscS inactivation observed under depolarizing conditions. The "break" point in this dependence corresponds to the voltage (-40 mV) where substates become dominant (compare Fig. 6 B and Fig. 3 A). This coincidence suggests that the leftmost part of the $\tau(V)$ dependence likely reflects the rate of transitions between the substates (S) and the inactivated state (I) but not a direct inactivation from the open (O) state. The slope thus reflects the decrease of the activation barrier for the S→I transition on voltage. Estimation shows that this process corresponds to an outward transfer of approximately two positive charges per heptamer across the entire electric field. If one elementary charge per subunit (seven charges total) were moving outward, the effective displacement of charges within the membrane from the S state to the transition state between the S and I states (top of the barrier) would be ~5 Å. This displacement would be smaller if more charges were engaged.

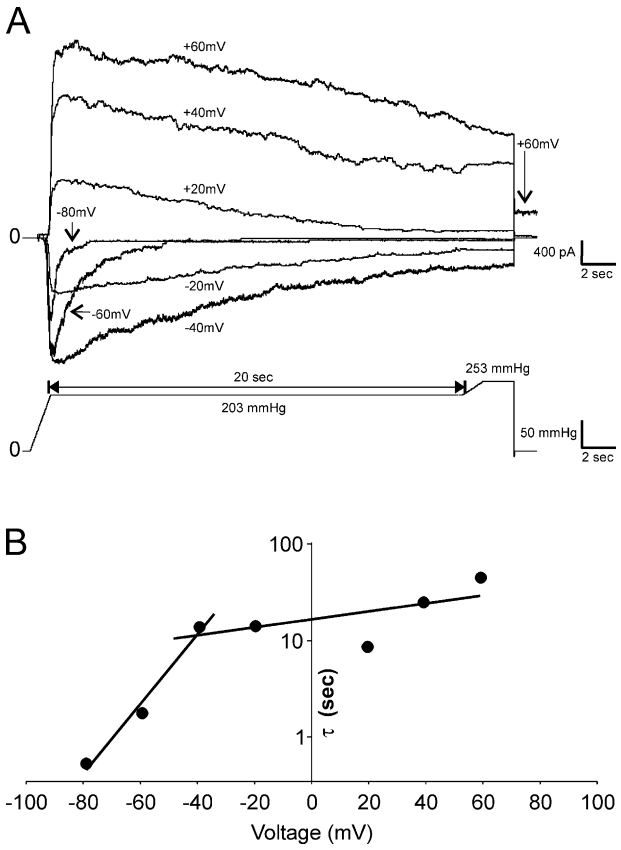

FIGURE 6. MscS inactivation is faster at depolarizing voltages. (A) Traces recorded with the prepulse pressure protocol at pipette voltages from -80 to $+80$ mV. The falling phase was fitted with a single exponent. (B) The characteristic time of inactivation as a function of pipette voltage. The high slope of the left part of the dependence corresponds to the barrier reduction equivalent to the energy of two positive charges ($q = +2$) per complex transferred outwardly across the entire transmembrane field.

DISCUSSION

We presented here electrophysiology recordings and analysis that illustrate the behavior of MscS in its native setting. In some instances, the protein was overexpressed two to four times compared with its density in wild-type *E. coli* strains via an induction the P_{lacUV5} promoter. Where single channel analysis was desired, a low level of MscS expression, close to wild-type density, was achieved through promoter leakage, without induction. The MJF465 triple knockout (*mscL*$^-$, *mscS*$^-$, *mscK*$^-$) *E. coli* host strain excluded any potential interference from other endogenous mechanosensitive channels. The pressure-clamp apparatus provided a critical advantage in terms of precision and reproducibility of stimulation by ramps of pressure, and the custom-written software HISTAN streamlined generation of multiple dose–response curves.

The major traits of MscS observed in situ can be reiterated as follows. The transition from the closed to fully open state (C→O) displays a steep dependence on membrane tension with an apparent mechanotransduction area of ~18 nm^2. The fully open state is stable at high tensions (and at moderate voltages), however at tensions below the activation midpoint ($\gamma_{1/2}$), the channel tends to inactivate within tens of seconds. Thus, under slow application of pressure, the resultant channel activity is much lower than with an abruptly applied stimulus of the same amplitude. The inactivated state of MscS is nonconductive and long lived. The complete return from the inactivated (refractory) to the closed state (I→C) takes at least 3 min. The main closed-to-open transition (C→O) is essentially voltage independent. However, at negative pipette (depolarizing) voltages <-40 mV and strong positive pipette (hyperpolarizing) voltages $>+80$ mV, MscS tends to occupy subconducting states (Fig. 3 A). Depolarizations beyond -40 mV strongly promote transitions to the subconducting states (O→S) followed by inactivation (S→I). While channel activation (C→O) was always observed as an instant conductance increase (at a given recording bandwidth), signifying a fast and concerted conformational change (Shapovalov and Lester, 2004), inactivation broken up into subtransitions appears to be a less cooperative event. The rate of inactivation exponentially increases with depolarizing voltage and decreases with tension. The gating characteristics of MscS are similar in KCl and NaCl buffers.

The presented phenomenology of MscS gating is different from what was depicted in early studies. The very first report by Martinac et al. (1987) described a 1-nS channel activated at pipette pressures of 40–60 mm Hg, considerably lower than those we used to activate MscS (140–300 mm Hg). The open probability for these channels markedly increased at depolarizing voltages, which we do not observe for MscS. The channel was active in KCl, but practically inactive in NaCl, a property later ascribed to MscK (Li et al., 2002). We acknowledge that at the time of the study it was difficult to separate the activities of these two different species, MscS and MscK. The characteristic propensity of MscS to time-dependent inactivation, however, suggests that the quasi-equilibrium traces recorded for minutes presented by Martinac et al. belonged mostly to MscK. The inactivation of the small (1 nS) channels taking place specifically at intermediate pressures was well documented by Koprowski and Kubalski (1998), however, these experiments covered only a narrow range of potentials (+30 to −30 mV), which precluded observation of the steep voltage dependence at stronger depolarizations described above.

The presented phenomenology of MscS also helps us to interpret the crystal structure (Bass et al., 2002). The crystal structure of MscS revealed a de-lipidated protein complex with TM1 and TM2 helices splayed at an unusual 30° angle relative to the membrane normal. The protein surface displayed conspicuous gaps between the TM1–TM2 pairs and the pore-forming TM3 helices, which should be either hydrated or filled with lipid (if such a conformation occurs in the native membrane). It is possible that the native resting conformation of MscS packs the TM1–TM2 pairs more tightly against the central pore, forming a more compact barrel. Indeed, in the absence of direct interactions between TM1–TM2 and TM3, it is unclear how tension developing in the lipid bilayer could be transmitted from the lipid-facing protein surface to the pore. Our preliminary steered molecular dynamic (SMD) simulations indicated that the swinging motion of the TM1–TM2 bundle about the extracellular hinge (G90 and adjacent residues) is essentially unrestrained. A gentle pressure, constricting the barrel from the outside, could then restore the contacts between TM2 and TM3 (unpublished data).

Despite initial conclusion that the crystal structure represents the open state (Bass et al., 2002), our computational analysis suggested that the pore in the crystal structure is largely dehydrated and must be nonconductive (Anishkin and Sukharev, 2004). The estimations showed that the pore constriction, with a water-accessible lumen of ~7 Å in diameter, must be expanded by at least 8 Å to conduct at 1 nS as measured in experiments. The dehydrated pore and the uncoupled state of the peripheral helices from the pore-forming helices suggest that the channel, in this particular conformation, would not only be nonconductive but also irresponsive to tension applied to its periphery, the functional definition of an inactivated state. We believe that the overall structure, represented in the crystal, is a conformation which likely resembles the inactivated state of MscS. Based on these considerations and the phenomenology above, we propose the following kinetic scheme and mechanism of MscS gating.

The scheme presented in Fig. 7 A shows positions of the main states in the area-charge plane. The solid arrows represent transitions observed frequently at moderate pipette voltages. Dashed lines depict transitions, involving substates, favored by moderate to high negative pipette voltages. Dotted lines represent possible transitions, which appeared infrequently, and have therefore not been characterized. An example of a dotted transition is the "silent" inactivation of the channel directly from the closed state. This transition seems to occur during prolonged exposures of the channel population to subthreshold tensions. We also cannot eliminate the possibility of a small number of channels returning to the open state (O) from the inactivated state (I). However, the probability of such a transition appears to be extremely low. The most common pathway from the inactivated state back to the closed state was a slow return favored by low tension and positive pipette voltages. Direct transitions from the fully open to the inactivated state were observed most frequently in traces at low to moderate positive voltages. Although we observed this pathway as a straight transition (O→I), the frequency response of our recordings was insufficient to exclude a composite (O→S→I).

The main rightward transition from the closed (C) to open (O) state is accompanied by a substantial area change but almost no charge transfer as the gating charge associated with the C→O transition was estimated to be only +0.8 per complex or +0.1 per subunit. We presume that in the resting state, the barrel has a compact conformation with all transmembrane helices tightly packed around the pore. The opening is achieved through a concerted outward movement of helices, which results in wetting and expansion of the pore constriction. The absence of voltage dependence at this stage signifies that the charges on the outer "voltage-sensing" helices (R46, R54, R59, K60, R74, as well as D62 and D67) do not experience any net transmembrane movement. TM1 and TM2 likely remain associated with the TM3 helices in the barrel, moving laterally. A cartoon representation of the transition from the closed to the open state is illustrated in Fig. 7 B.

The data presented in Figs. 2, 3, and 6 show that depolarizing voltages favor transitions to subconducting states followed by the inactivated state. The fact

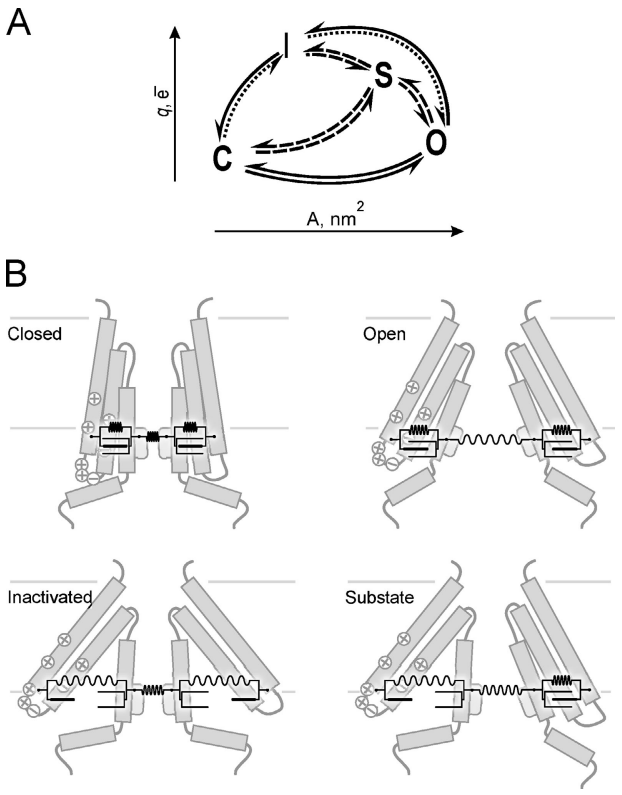

FIGURE 7. The hypothetical gating mechanism of MscS. (A) Kinetic scheme of MscS transitions presented on an area-charge plane shows transitions frequently observed at low voltages (solid lines), transitions favored by negative pipette voltages beyond −40 mV (dashed lines), and transitions which are possible but have not been characterized (dotted lines). The distances between the main states (closed, C; open, O; substate, S; and inactivated, I) reflect the changes of in-plane area (ΔA) and transmembrane movement of charges (Δq) associated with each transition. (B) Cartoon representation of helical positions associated with each state. An effective dashpot between the peripheral TM1–TM2 bundle and the pore-forming TM3 allows pore helices to disengage and collapse into a closed conformation, causing inactivation. A small upward swing of the peripheral helices generates gating charge associated with inactivation.

that the channel enters the inactivated state (I) typically through a substate (S) led us to infer that substates are structural intermediates between the open and inactivated states. We therefore placed these states on the area-charge plane in sequence with increasing q. We presume that under depolarizing conditions, the outwardly directed electric field acts on the charged residues residing in TM1 and TM2, pushing the helices toward the extracellular side and thus favoring their detachment from the core TM3 helices. This uncoupling, associated with an upward swinging motion, generates gating charge and stipulates voltage dependence. At the same time, the TM3 helices collapse back to a narrow-pore conformation, which eventually causes dehydration of the constriction and return to a nonconductive state. This mechanism of combined activation and inactivation performed by a single gate, and involving hinged motion of the inner helices, is similar to the inactivation mechanism proposed for the voltage gated channel NaChBac (Zhao et al., 2004). The substates may represent intermediate states in this pathway with only a few subunits having detached TM1–TM2 pairs and a partially collapsed pore. The fully inactivated state is achieved when this process of helix decoupling completes, resulting in formation of the characteristic crevices on the cytoplasmic side of the channel seen in the crystal structure. The conformations of an "asymmetric" substate and the inactivated state are schematically illustrated in Fig. 7 B. Whether these crevices are filled with water or lipid is unclear, but the slow return from the inactivated to the closed state may be limited by slow lipid diffusion out of the confined crevice. Furthermore, this return would be aided by the charges on the TM1 and TM2 helices as the bacterium reenergizes its membrane.

The kinetic data presented in Fig. 6 was insufficient to conclude the entire gating charge associated with inactivation because we only measured the increase in rate of the O→I transition on voltage, but not the equilibrium probability distribution. However, the data indicated that this increase in the rate of inactivation must be accompanied by a decrease in the transition barrier equivalent to the energy of transferring two positive charges across the entire electric field. If we assume that only one charge per subunit is engaged in inactivation, then all seven charges per complex have to move by ∼5 Å across the bilayer. If three charges per subunit are involved (the net charge of each peripheral pair of helices is +3), only 1.7 Å of displacement is necessary to reach the transition state leading to inactivation. This estimate seems to be consistent with the expected moderate scale of the TM1–TM2 helices swing.

Fig. 4 illustrates full activation of MscS on a steep application of pressure but strongly attenuated responses to slow ramps. The fact that the midpoint of activation does not change with the speed of ramp suggests that opening is not impeded by channel kinetics within the studied time frame. The lower total activity observed with a slow ramp is apparently due to MscS inactivation at intermediate tensions near the midpoint. Since this process was observed at all voltages, it can be assumed that the inactivated state of the channel is the lowest energy state at intermediate tensions. At negative pipette voltages, a low-barrier passage is opened to the inactivated state through the substates. How then does high tension stabilize the open state? Although we cannot exclude the possibility that high membrane tensions kinetically trap the open state of MscS, it is more likely that under such conditions, the open conformation represents a true energetic minimum. If the effective in-plane area of the open state were larger than

that of the inactivated state (as denoted in the area-charge plane, Fig. 7 A), at high tension, the energy of the open state would be lower than that of inactivated state. The concerted expansion of TM1, TM2, and TM3 associated with the C→O transition, during which the protein retains a tight packing of these transmembrane helices, brings a substantial increase of the channel footprint in the lipid bilayer. The area increase for this transition is estimated to be 18 nm^2 from dose–response curves (Fig. 1). An activating tension of 7 dyne/cm would result in an energetic stabilization of the open state of ~30 kT. In contrast, the O→I transition likely results in a decrease of the effective in-plane area of the channel. The decoupling of TM1–TM2 pairs from the core helices and their subsequent spreading creates slits and crevasses critically changing the protein outline in the plane of the membrane. Lipids may penetrate into the slits, taking a part of the protein area and thus reducing the effective lipid-excluded area of the protein. In this way, spreading of helical pairs and "intermixing" with the surrounding lipids explains the effective decrease of the in-plane area as a result of transitions into the subconducting and inactivated states. With increasing tension, the inactivation rate decreases (Fig. 5 B, inset) and the slope suggests that the transition state leading to inactivation has 10.6 nm^2 smaller in-plane area than the open state. This implies that the area difference between the end states (O and I) is even larger.

The ability of MscS to reversibly inactivate may be one of the features that allow it to respond differently to various environmental parameter changes. Indeed, the total channel population responds in full when stimulated by a high pressure applied abruptly, but largely inactivates during the slow passage through a narrow region of pressures below the midpoint. The quick reaction to an abrupt stimulus and "dumping" of a slowly applied force resembles a "dashpot": a velocity-sensitive viscous element that would connect the gate of the channel to the tension-receiving protein interface (Fig. 7 B). This dashpot functionality may be ascribed to the postulated contacts between the pore-forming (TM3) and peripheral helices (TM1 and TM2) capable of disengaging and allowing lipid penetration.

This mechanism that makes MscS susceptible to a sudden pressure onset, but allows it to "ignore" slowly applied stimuli, may be important in environmental situations where rehydration of cells occurs gradually and nonselective release of osmolytes is not desirable. Instead of simply jettisoning the solutes through opening, the channel inactivates giving time to other osmoregulatory systems to release some of the solutes in a more selective manner or exchange them (Wood, 1999). Because the time course of pressure buildup depends on water permeability, there is a possible functional interplay of MscS with aquaporins previously discussed in Booth and Louis (1999). It would be interesting to test the osmotic rescuing function of MscS in *aqpZ*$^-$ strains. Previously, MscS and MscL have been shown to be redundant in *E. coli* (Levina et al., 1999). However, the evolutionary preservation of the two channel species suggests that they are not interchangeable in certain environmental situations. In fact, after a gradual change of pressure, all MscS may be inactivated, and only noninactivating MscL would be capable of fulfilling the "safety valve" function. The described kinetics now suggests several enticing possibilities for the study of MscS under different dynamic conditions of osmotic shock.

The authors would like to thank Dr. Ian R. Booth for the MJF465 strain and Dr. Paul Blount for the MscS clone used in these experiments.

This work was supported by National Aeronautics and Space Administration and National Institutes of Health research grants to S. Sukharev.

Olaf S. Andersen served as editor.

Submitted: 22 October 2004
Accepted: 9 December 2004

REFERENCES

Anishkin, A., and S. Sukharev. 2004. Water dynamics and dewetting transitions in the small mechanosensitive channel MscS. *Biophys. J.* 86:2883–2895.

Bass, R.B., P. Strop, M. Barclay, and D.C. Rees. 2002. Crystal structure of *Escherichia coli* MscS, a voltage-modulated and mechanosensitive channel. *Science.* 298:1582–1587.

Besch, S.R., T. Suchyna, and F. Sachs. 2002. High-speed pressure clamp. *Pflugers Arch.* 445:161–166.

Blount, P., and P.C. Moe. 1999. Bacterial mechanosensitive channels: integrating physiology, structure and function. *Trends Microbiol.* 7:420–424.

Booth, I.R., and P. Louis. 1999. Managing hypoosmotic stress: aquaporins and mechanosensitive channels in *Escherichia coli. Curr. Opin. Microbiol.* 2:166–169.

Chiang, C.S., A. Anishkin, and S. Sukharev. 2004. Gating of the large mechanosensitive channel in situ: estimation of the spatial scale of the transition from channel population responses. *Biophys. J.* 86:2846–2861.

Cui, C., and J. Adler. 1996. Effect of mutation of potassium-efflux system, KefA, on mechanosensitive channels in the cytoplasmic membrane of *Escherichia coli. J. Membr. Biol.* 150:143–152.

Jiang, Y., V. Ruta, J. Chen, A. Lee, and R. MacKinnon. 2003. The principle of gating charge movement in a voltage-dependent K^+ channel. *Nature.* 423:42–48.

Koprowski, P., and A. Kubalski. 1998. Voltage-independent adaptation of mechanosensitive channels in *Escherichia coli* protoplasts. *J. Membr. Biol.* 164:253–262.

Koprowski, P., and A. Kubalski. 2003. C termini of the *Escherichia coli* mechanosensitive ion channel (MscS) move apart upon the channel opening. *J. Biol. Chem.* 278:11237–11245.

Levina, N., S. Totemeyer, N.R. Stokes, P. Louis, M.A. Jones, and I.R. Booth. 1999. Protection of *Escherichia coli* cells against extreme turgor by activation of MscS and MscL mechanosensitive channels: identification of genes required for MscS activity. *EMBO J.*

18:1730–1737.

Li, Y., P.C. Moe, S. Chandrasekaran, I.R. Booth, and P. Blount. 2002. Ionic regulation of MscK, a mechanosensitive channel from *Escherichia coli*. *EMBO J.* 21:5323–5330.

Martinac, B., M. Buechner, A.H. Delcour, J. Adler, and C. Kung. 1987. Pressure-sensitive ion channel in *Escherichia coli*. *Proc. Natl. Acad. Sci. USA*. 84:2297–2301.

Miller, S., M.D. Edwards, C. Ozdemir, and I.R. Booth. 2003. The closed structure of the MscS mechanosensitive channel. Cross-linking of single cysteine mutants. *J. Biol. Chem*. 278:32246–32250.

Okada, K., P.C. Moe, and P. Blount. 2002. Functional design of bacterial mechanosensitive channels. Comparisons and contrasts illuminated by random mutagenesis. *J. Biol. Chem.* 277:27682–27688.

Pivetti, C.D., M.R. Yen, S. Miller, W. Busch, Y.H. Tseng, I.R. Booth, and M.H. Saier Jr. 2003. Two families of mechanosensitive channel proteins. *Microbiol. Mol. Biol. Rev.* 67:66–85.

Sachs, F. 1992. Stretch-sensitive ion channels: an update. *Soc. Gen. Physiol. Ser.* 47:241–260.

Shapovalov, G., and H.A. Lester. 2004. Gating transitions in bacterial ion channels measured at 3 micros resolution. *J. Gen. Physiol.* 124:151–161.

Sotomayor, M., and K. Schulten. 2004. Molecular dynamics study of gating in the mechanosensitive channel of small conductance MscS. *Biophys J.* 87:3050–3065.

Sukharev, S. 2002. Purification of the small mechanosensitive channel of *Escherichia coli* (MscS): the subunit structure, conduction, and gating characteristics in liposomes. *Biophys. J.* 83:290–298.

Sukharev, S.I., W.J. Sigurdson, C. Kung, and F. Sachs. 1999. Energetic and spatial parameters for gating of the bacterial large conductance mechanosensitive channel, MscL. *J. Gen. Physiol.* 113: 525–540.

Vasquez, V., and E. Perozo. 2004. Voltage dependent gating in MscS. *Biophys. J.* 86:545a.

Wood, J.M. 1999. Osmosensing by bacteria: signals and membrane-based sensors. *Microbiol. Mol. Biol. Rev.* 63:230–262.

Zhao, Y., V. Yarov-Yarovoy, T. Scheuer and W.A. Catterall. 2004. A gating hinge in Na^+ channels; a molecular switch for electrical signaling. *Neuron.* 41:859–865.